LETTER

Maskless and Resist-Free Rapid Prototyping of Three-Dimensional Structures Through Electron Beam Induced Deposition (EBID) of Carbon in Combination with Metal-Assisted Chemical Etching (MaCE) of Silicon

Konrad Rykaczewski,[†] Owen J. Hildreth,[‡] Dhaval Kulkarni,[‡] Matthew R. Henry,[†] Song-Kil Kim,[†] Ching Ping Wong,[‡] Vladimir V. Tsukruk,[‡] and Andrei G. Fedorov*[,†]

G. W. Woodruff School of Mechanical Engineering and School of Materials Science and Engineering, Georgia Institute of Technology, Atlanta, GA 30332

ABSTRACT In this work, we introduce a maskless, resist-free rapid prototyping method to fabricate three-dimensional structures using electron beam induced deposition (EBID) of amorphous carbon (aC) from a residual hydrocarbon precursor in combination with metal-assisted chemical etching (MaCE) of silicon. We demonstrate that EBID-made patterned aC coating, with thickness of even a few nanometers, acts as a negative "mask" for the etching process and is sufficient for localized termination of the MaCE of silicon. Optimal aC deposition settings and gold film thickness for fabrication of high-aspect-ratio nanoscale 3D silicon structures are determined. The speed necessary for optimal aC feature deposition is found to be comparable to the writing speed of standard Electron Beam Lithography and the MaCE etching rate is found to be comparable to standard deep reactive ion etching (DRIE) rate.

KEYWORDS: nanofabrication • metal-assisted chemical etching • silicon • 3D nanostructures • electron beam induced deposition • amorphous carbon • residual hydrocarbons

Silicon nanostructures can be made in numerous ways and are important to a variety of applications such as electronic devices (1), photovoltaic cells (2), optoelectronics (3), microelectromechanical systems (MEMS) (4), chemical and biological sensors (5−7), and through-wafer interconnects (8). Standard fabrication techniques include wet chemical methods, utilizing liquid acids and bases, and dry chemical methods such as plasma etching, ion etching, and deep reactive ion etching (DRIE). Although these technologies have successfully been used to fabricate structures of varying degrees of complexity, maintaining a high aspect ratio of produced structures becomes increasingly difficult as feature sizes shrink into the nanoscale. Morton et al. (9) have recently demonstrated that the maximum aspect ratio of silicon nanowires achievable with DRIE fabrication can be pushed from ∼10:1 to ∼50:1; however, the process leaves rough and scalloped sidewalls.

Metal-assisted chemical etching (MaCE) of silicon has been recently applied to fabrication of high-aspect-ratio silicon nanowires (10−13) and three-dimensional silicon nanostructures (14, 15) with smooth and non-scalloped walls. In MaCE, a metal catalyst such as Ag, Au, or Pt is deposited onto a silicon surface as either nanoparticles or a discontinuous thin film that locally increases the silicon dissolution rate in an etchant solution of hydrofluoric acid (HF) and hydrogen peroxide (H_2O_2) or other oxidizing agent. The etching process begins as H_2O_2 is catalytically reduced on the metal surface, creating a local cathode on the etchant side of the metal that injects holes (h^+) into the valence band of silicon, leading to a hole (h^+) rich region of silicon (Si*) surrounding the metal catalyst. The holes (h^+) are consumed at the HF/Si* interface in oxidation of Si^0 to Si^{4+} producing soluble SiF_6^{2-} and H_2SiF_6 (16). The etching process continues as metal nanoparticles or structures travel into the regions where the silicon was removed, forming a moving cathodic interface as the silicon is dissolved. Dependent on etchant composition, silicon dissolution can be confined to a region in close proximity to the catalyst particle (creating high aspect ratio nearly vertical protrusions into silicon) or can take place over a wide region around the catalyst particle (creating conical holes) (10, 17).

Area-selective MaCE of silicon has been achieved by patterning metal nanoparticles and thin films using colloidal crystal templating (18, 19), photo- and electron beam-lithography (14, 15), microcontact imprinting (20), and focused ion beam deposition (FIBD) (21). Best results for nanoscale pattern transfer have been achieved so far by metal patterning using electron beam lithography (14, 15). However, the etching direction of the metal patterns is difficult to control and significant deformation of the metal

* Corresponding author.
Received for review January 28, 2010 and accepted March 29, 2010
[†] G. W. Woodruff School of Mechanical Engineering, Georgia Institute of Technology.
[‡] School of Materials Science and Engineering, Georgia Institute of Technology.
DOI: 10.1021/am1000773
© 2010 American Chemical Society

LETTER

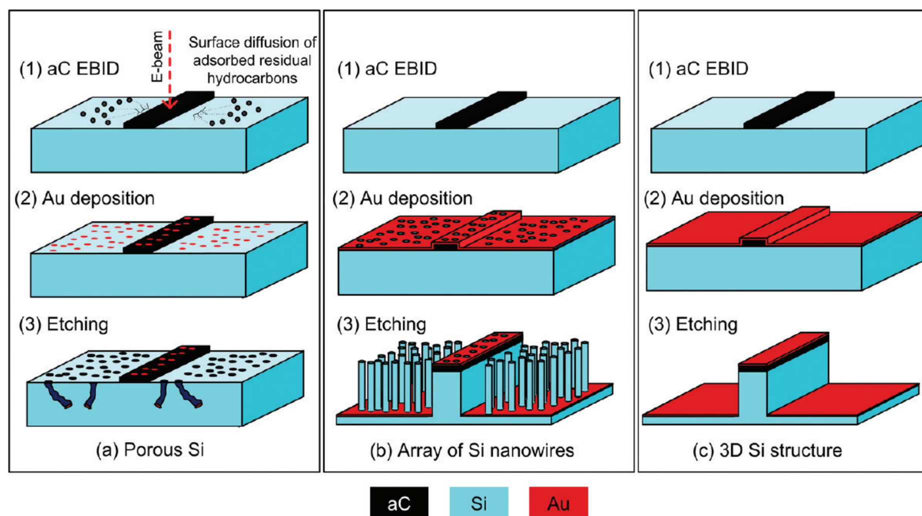

FIGURE 1. Schematic of steps involved in fabrication of EBID aC/MaCE patterns of (a) porous silicon from discrete nanoparticles, (b) silicon nanowires from discontinuous metal films or high density nanoparticle layers, and (c) 3D silicon nanostructures from slightly discontinuous metal films.

structures can occur during the etching process (14). In this work, we demonstrate that a very thin layer of amorphous carbon (aC) formed using EBID underneath of a metal surface (see Figure 1a) is sufficient for localized blocking of the MaCE of silicon and acts as a negative "mask" for the etching process. Additionally, we determine the gold film thicknesses necessary for fabrication of either EBID-patterned porous silicon (with deposition of Au particles, see Figure 1a), or EBID-patterned silicon nanowires (with deposition porous Au film, see Figure 1b), or EBID-patterned solid 3D silicon nanostructures (with deposition of almost continuous Au film, see Figure 1c).

In the EBID process, a solid amorphous carbon deposit is formed at the point of impact of a focused primary electron beam due to interaction of backscattered primary and secondary electrons with surface adsorbed residual hydrocarbons (22, 23). In surface imaging, EBID of amorphous carbon from residual hydrocarbons is a common contamination problem that has been recognized since the early days of electron microscopy (24−27). However, with appropriate electron beam control this "parasitic" microscopy process can provide a basis for 3D nanofabrication (28) and nanoscale metrology (29, 30). One of the primary advantages of EBID of aC from residual hydrocarbons is that it is maskless, resist-free, can be performed in any unmodified electron microscope. Here, we demonstrate that the deposition speed of aC structures optimal for the developed fabrication technique is comparable to the writing speed of electron beam lithography.

All samples are prepared on a single-side-polished p-type (1−100Ω cm) single crystal (100) silicon wafer cleaned using a 4:1 piranha solution of H_2SO_4:H_2O_2 and then a dilute HF (1:100). The EBID aC structures are fabricated using a tungsten filament Quanta 200 ESEM by passing the electron beam along the surface and locally dissociating surface-adsorbed residual hydrocarbons. An electron beam energy of 30 keV, current of ~24 pA, and diameter of ~40 nm with background (chamber) pressure of $\sim 1 \times 10^{-5}$ Torr is used. Amorphous carbon Georgia Tech (GT) logo structures are fabricated using Nanometer Pattern Generation System v8 from J.C. Nabity Lithography Systems with center-to-center and line distances of 2 nm, lines doses in the 12−1200 μC/m range, and 1, 10, and 100 pattern passes (corresponding to 21 to 2.1 second refresh times for 10 and 100 repetitions). The Au films are sputtered using Denton Vacuum Desk IV sputterer at a pressure of 50 mTorr for 60, 120, 140, and 160 seconds. The corresponding average film thicknesses of 3.5, 6.7, 8.2, and 9.1 nm are determined from thickness measurements at several locations of a sample using a Woolam M2000U spectroscopic ellipsometer equipped with WVASE32 modeling software (31) with resolution of ±0.5 nm. All structures are etched in a mixture of 4 mL of HF (Aldrich, 49%), 1.2 mL of H_2O_2 (Aldrich, 30%), and 1.7 mL of H_2O (distilled) for 15 or 30 seconds. The dimensions and morphology of the structures are characterized using scanning electron microscope (SEM) and atomic force microscopy (AFM). The AFM imaging was performed using DI 3000 in light tapping mode with silicon tips (Mikromasch) with a spring constant of 42 N/m and resonance frequency of ~360 kHz (31, 32).

Figure 2a shows results of EBID-aC-patterned GT logos deposited under varied conditions followed by sputtering of 6.7 nm of Au and 30 seconds of etching in the HF/H_2O_2/H_2O solution. MaCE of the aC/Au-coated samples results in localized etching of silicon where a metal catalyst is in direct contact with Si, producing clearly distinguishable arrays of Si nanowires (see Figure 3b) everywhere but in the areas defined by the aC patterns (11−13). In essence, the nonconductive aC (33−35) underfill beneath the gold layer blocks hole injection into silicon, which is needed for the etching process to proceed, thus making a "negative" mask for MaCE. Higher EBID line doses result in detrimental and non-localized aC build-up due to residual hydrocarbon dissociation by backscattered electrons (BSE) and secondary electrons (SE) generated far away from impact of the primary electrons (PE) (22, 23). The non-localized aC deposi-

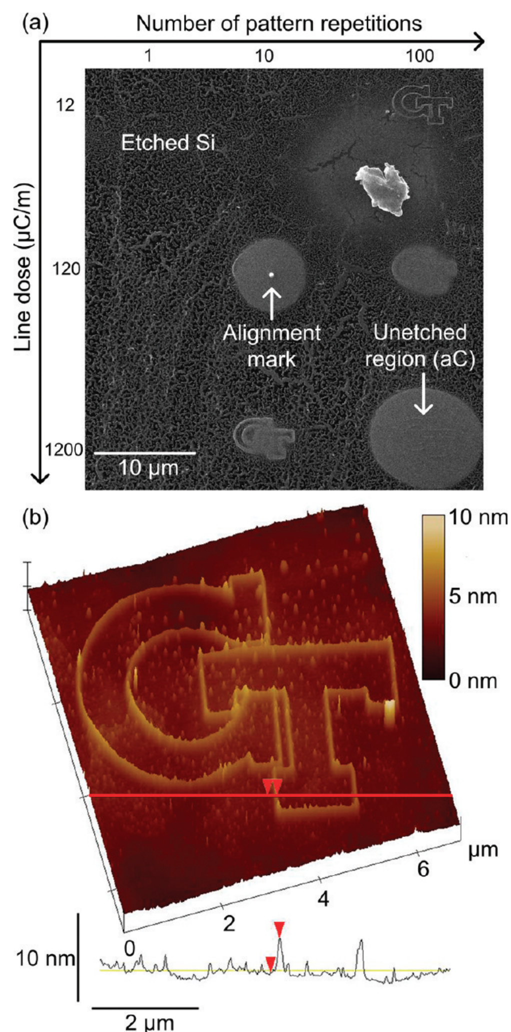

FIGURE 2. (a) SEM image of post 30 second MaCE of 6.7 nm thick Au film with eight underlying EBID aC GT logos, acting as the negative masks, and alignment mark deposited with varied line doses and number of repetitions (refresh times), and (b) AFM topographical map of EBID aC-patterned GT logo deposited with line dose of 90 μC/m with 100 pattern repetitions (refresh time of 2.1 s), resulting in maximal line height of ~4 nm and width of ~150-200 nm.

tion is readily observed as unetched circular regions in the bottom right corner in Figure 2a. Furthermore, the ~5 μm radius of the unetched circular region corresponds well to the 5−6 μm radius of the 30 keV PE interaction volume in bulk silicon (36). Optimal conditions for fabrication of high-resolution aC deposits are achieved by repeating exposure of a pattern with a lower line dose rather than a single exposure because the in-between exposure time (refresh time) allows for replenishment of depleted precursor into the deposition zone through surface diffusion (23, 37−39). This effect is clearly demonstrated by comparing results of deposition with the same total line dose of 1200 μC/m, but administered in a single pass (bottom left corner of Figure 2a shows no unetched features of GT logo) and in 100 passes (top right corner of Figure 2a clearly shows an unetched GT logo). The AFM image in Figure 2b shows the morphology and dimensions of an optimized aC-masked GT logo deposited with per-pass line dose of 90 μC/m and 100 pattern repetitions (refresh time of 2.1 s) of EBID, resulting in a

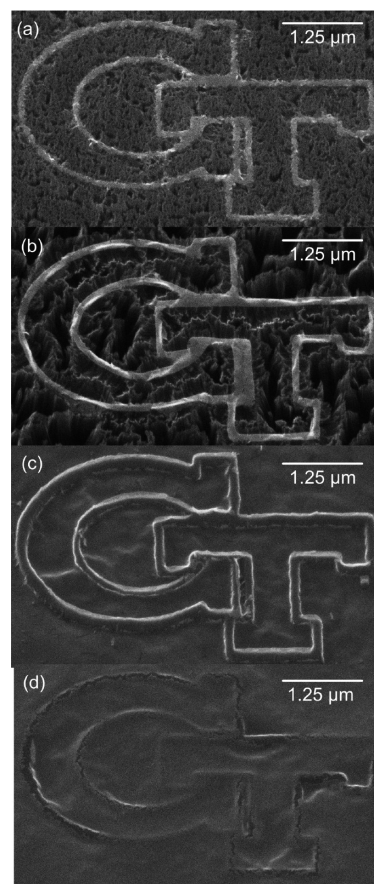

FIGURE 3. SEM images (under 30° tilt) of structures formed after 15 seconds of etching of EBID-aC/Au-coated samples with Au film thicknesses of 3.5, 6.7, 8.2, and 9.1 nm in $HF/H_2O_2/H_2O$ solution.

maximum line height of ~4 nm and a width of ~150−200 nm. For these settings, the total per-pixel electron dose required for aC deposition (~1.2 × 10^7 electrons/pixel) is comparable to per-pixel electron dose (5.0 × 10^7) used for high-resolution electron beam lithography (40), thus resulting in similar deposition/writing speeds for the two processes.

Next we determine the influence of the Au film thickness on the resulting structure and morphology of the etched silicon and produced patterns as defined by aC structures shown in Figure 2b. Figure 3 summarizes the effect of etching Au films with thickness of 3.5 nm (Figure 3a), 6.7 nm (Figure 3b), 8.2 nm (Figure 3c), and 9.1 nm (Figure 3d), in the presence of underlying aC structures, for 15 seconds. While the aC structure successfully acts as a negative etching mask for all Au layer thicknesses, the morphology of etched silicon varies greatly with the Au layer thickness. The thinnest Au coating of 3.5 nm results in deposition of discrete Au nanoparticles, which etch in random direction forming porous silicon (diagram in Figure 1a and experimental results in Figure 3a) (41). Increasing the Au coating thickness to 6.7 nm results in merging of the Au particles into a dense, but still discontinuous (porous) Au film with sufficiently high Au particle density (42) to allow for formation of arrays of silicon nanowires during the etching process (diagram in Figure 1b and experimental results in Figure 3b) (12, 13, 17). The Au coating thickness of 8.2 nm results in a sufficient decrease in porosity of the Au layer to prevent the formation

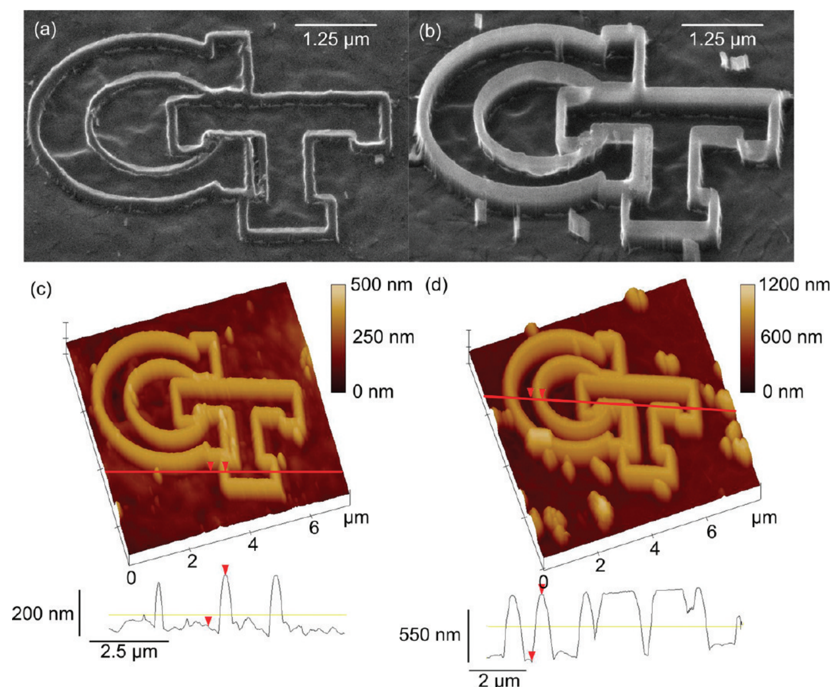

FIGURE 4. SEM images (under 30° tilt) and AFM topological maps of Si structures formed after (a, c) 15 and (b, d) 30 s of etching of EBID-aC/Au-coated samples (Au film thicknesses is 8.2 nm).

of nanowires, but still allows sufficient penetration of the etchant solution to produce the desired rapid and spatially uniform etching of the silicon (diagram in Figure 1c and experimental results in Figure 3c) (14). As shown in Figure 3d, a further increase in the thickness of an Au film results in deposition of fully-dense, continuous metal film preventing any significant etching of the silicon.

The AFM and SEM topological images of structures formed after 15 and 30 seconds of etching of the EBID-aC/Au-coated samples with aC (Figure 2b) and Au (Figure 3c) deposition settings are shown in Figure 4. Etching for 15 and 30 s resulted in removal of ∼225 nm and ∼700 nm of silicon, respectively. The resulting etching rate of ∼1.4 μm/min is comparable to the typical DRIE etching rate of 1.5−4 μm/min (43). The attained line widths are in the 80−120 nm and 120−150 nm range for the porous/nanowire and solid 3D silicon structures, respectively.

Decreased line widths on porous/nanowire silicon are due to the fact that nanoparticles etch in random directions and thus can undercut the aC pattern. Line widths of 120−150 nm of the solid 3D structures (Figure 4) correspond well to the 150−200 nm aC line widths as deposited by EBID (Figure 2b). The fabricated aC lines are 2−3 wider than the electron beam diameter (∼40 nm) due to surface mass transport effects (22), scattering of SE from the sides of deposits (44), and non-idealities such as electron beam and sample stage drift during the ESEM operation. However, further optimization of conditions such as use of a field emission SEM instrument with smaller beam diameters (sub-1 nm) and greater beam current would allow for EBID fabrication of sub-10 nm aC mask features and should result in an improved resolution of MaCE-etched Si nanostructures (28, 45, 46).

In conclusion, in this work, we introduce a maskless and resist-free rapid prototyping method for making three-dimensional structures using Electron Beam Induced Deposition (EBID) of amorphous carbon (aC) from residual hydrocarbons in combination with Metal-assisted Chemical Etching (MaCE) of silicon. We demonstrate that a 3−4 nm tall EBID-aC-made barrier layer is sufficient for localized blocking of the MaCE of silicon, yielding a negative masking process for nanostructure fabrication. EBID settings of per-pass line dose of 90 μC/m and 100 pattern repetitions with a refresh time of 2.1 s, in combination with ∼8 nm thick Au layer for MaCE, are found to be optimal process parameters for fabrication of solid 3D silicon nanostructures with sharp edges and straight walls. It is important to note that the morphology of the Au layer is highly dependent on the film deposition method and may have an impact on the MaCE process. Thus, the optimal Au layer thickness might be dependent on the Au layer fabrication process, and in practice should be obtained through a simple calibration procedure introduced in this work. The speed of optimal aC feature deposition is found to be comparable to the writing speed of electron beam lithography, and the MaCE etching rate is found to be in the range of etching rates of DRIE. Thus, a hybrid EBID-MaCE process developed in this work is as fast in pattern definition and etching speed as any alternative techniques, but, owing to its maskless and resist-free nature, it is significantly simpler, more flexible and robust as compared to the current state-of-the-art 3D nanofabrication techniques. Furthermore, the EBID-MaCE process also has potential for controllable pattern definition of sub-10 nm features that enable formation of high-aspect-ratio 3D nanostructures with smooth walls.

Acknowledgment. NSF Grant DMI 0403671 provided financial support for this work.

REFERENCES AND NOTES

(1) Ito, T.; Yamada, T.; Inao, Y.; Yamaguchi, T.; Mizutani, N.; Kuroda, R. *Appl. Phys. Lett.* **2006**, *89* (3), 3.
(2) Koynov, S.; Brandt, M. S.; Stutzmann, M. *Appl. Phys. Lett.* **2006**, *88* (20), 3.
(3) Weiss, S. M.; Haurylau, M.; Fauchet, P. M. *Opt. Mater.* **2005**, *27* (5), 740–744.
(4) Ben, Y.; Gianchandani, Y.; Peterson, G.; Bergsrom, P.; Li, G.; Plummer, D.; Borboni, A.; Ofdahl, L.; Sobhan, C.; Muntz, E., *MEMS Applications*; CRC: Boca Raton, FL, 2005.
(5) Brus, L. *J. Phys. Chem.* **1994**, *98* (14), 3575–3581.
(6) Lin, V. S. Y.; Motesharei, K.; Dancil, K. P. S.; Sailor, M. J.; Ghadiri, M. R. *Science* **1997**, *278* (5339), 840–843.
(7) Sailor, M. J.; Lee, E. J. *Adv. Mater.* **1997**, *9* (10), 783-&.
(8) Burkett, S. L.; Qiao, X.; Temple, D.; Stoner, B.; McGuire, G. *J. Vac. Sci. Technol., B* **2004**, *22* (1), 248–256.
(9) Morton, K. J.; Nieberg, G.; Bai, S.; Chou, S. Y. *Nanotechnology* **2008**, *19* (34), 345301.
(10) Tsujino, K.; Matsumura, M. *Electrochim. Acta* **2007**, *53*, 28–34.
(11) Peng, K. Q.; Hu, J. J.; Yan, Y. J.; Wu, Y.; Fang, H.; Xu, Y.; Lee, S. T.; Zhu, J. *Adv. Funct. Mater.* **2006**, *16* (3), 387–394.
(12) Huang, Z. P.; Fang, H.; Zhu, J. *Adv. Mater.* **2007**, *19* (5), 744.
(13) Huang, Z. P.; Zhang, X. X.; Reiche, M.; Liu, L. F.; Lee, W.; Shimizu, T.; Senz, S.; Gosele, U. *Nano Lett.* **2008**, *8* (9), 3046–3051.
(14) Hildreth, O. J.; Lin, W.; Wong, C. P. *ACS Nano* **2009**, *3* (12), 4033–4042.
(15) Chun, I. S.; Chow, E. K.; Li, X. L. *Appl. Phys. Lett.* **2008**, *92* (19), 3.
(16) Gorostiza, P.; Diaz, R.; Kulandainathan, M. A.; Sanz, F.; Morante, J. R. *J. Electroanal. Chem.* **1999**, *469* (1), 48–52.
(17) Chartier, C.; Bastide, S.; Levy-Clement, C. *Electrochim. Acta* **2008**, *53* (17), 5509–5516.
(18) Asoh, H.; Arai, F.; Ono, S. *Electrochem. Comm.* **2007**, *9* (4), 535–539.
(19) Asoh, H.; Arai, F.; Uchibori, K.; Ono, S. *Appl. Phys. Express* **2008**, *1* (6), 3.
(20) Harada, Y.; Li, X. L.; Bohn, P. W.; Nuzzo, R. G. *J. Am. Chem. Soc.* **2001**, *123* (36), 8709–8717.
(21) Chattopadhyay, S.; Bohn, P. W. *J. Appl. Phys.* **2004**, *96* (11), 6888–6894.
(22) Rykaczewski, K.; White, W. B.; Fedorov, A. G. *J. Appl. Phys.* **2007**, *101* (5), 054307.
(23) Rykaczewski, K.; Marshall, A.; White, W. B.; Fedorov, A. G. *Ultramicroscopy* **2008**, *108* (9), 989–92.
(24) Cosslett, V. E. *J. Appl. Phys.* **1947**, *18* (9), 844–845.
(25) Watson, J. H. L. *J. Appl. Phys.* **1947**, *18* (2), 153–161.
(26) Ellis, S. G. Paper read to American Electron Microscopy Society, Washington, D.C., November 1951.
(27) Ennos, A. E. *Br. J. Appl. Phys.* **1953**, (4), 101–106.
(28) Utke, I.; Hoffmann, P.; Melngailis, J. *J. Vac. Sci. Technol. B* **2008**, *26* (4), 1197–1276.
(29) Ding, W.; Dikin, D. A.; Chen, X.; Piner, R. D.; Ruoff, R. S.; Zussman, E.; Wang, X.; Li, X. *J. Appl. Phys.* **2005**, *98* (1),
(30) Kaplan-Ashiri, I.; Cohen, S. R.; Apter, N.; Wang, Y. K.; Seifert, G.; Wagner, H. D.; Tenne, R. *J. Phys. Chem. C* **2007**, *111* (24), 8432–8436.
(31) Tsukruk, V. V.; Reneker, D. H. *Polymer* **1995**, *36* (9), 1791–1808.
(32) Tsukruk, V. V. *Rubber Chem. Technol.* **1997**, *70* (3), 430–467.
(33) Miura, N.; Ishii, H.; Shirakashi, J.; Yamada, A.; Konagai, M. *Appl. Surf. Scie.* **1997**, *114*, 269–273.
(34) Kahng, Y. H.; Choi, J.; Park, B. C.; Kim, D. H.; Choi, J. H.; Lyou, J.; Ahn, S. J. *Nanotechnology* **2008**, *19* (19), 7.
(35) Rykaczewski, K.; Henry, M. R.; Kim, S.-K.; Fedorov, A. G.; Kulkarni, D.; Singamaneni, S.; Tsukruk, V. V. *Nanotechnology* **2009**, *21* (3), 035202.
(36) Joy, D. C. *Monte Carlo Modeling for Electron Microscopy and Microanalysis*; Oxford University Press: New York, 1995.
(37) Smith, D. A.; Fowlkes, J. D.; Rack, P. D. *Nanotechnology* **2008**, *19* (41), 11.
(38) Smith, D. A.; Fowlkes, J. D.; Rack, P. D. *Small* **2008**, *4* (9), 1382–1389.
(39) Amman, M.; Sleight, J.; Lombardi, D. R.; Welser, R. E.; Deshpande, M. R.; Reed, M. A.; Guido, L. J. *J. Vac. Sci. Technol., B* **1995**, *14* (1), 54–62.
(40) Vieu, C.; Carcenac, F.; Pepin, A.; Chen, Y.; Mejias, M.; Lebib, A.; Manin-Ferlazzo, L.; Couraud, L.; Launois, H. *Appl. Surf. Sci.* **2000**, *14*, 111–117.
(41) Li, X.; Bohn, P. W. *Appl. Phys. Lett.* **2000**, *77* (16), 2572–2574.
(42) Peng, K.; Lu, A.; Zhang, R.; Lee, S. T. *Adv. Funct. Mater.* **2008**, *18* (19), 3026–3035.
(43) Madou, M. J. *Fundametals of Microfabrication: The Science of Miniaturization*, 2nd ed.; CRC: Boca Raton, FL, 2002.
(44) Silvis-Cividjian, N. *Electron Beam Induced Nanometer Scale Deposition*; University of Delft: Delft, The Netherlands, 2002.
(45) Silvis-Cividjian, N.; Hagen, C. W.; Kruit, P. *J. Appl. Phys.* **2005**, *98* (8), 084905.
(46) Utke, I.; Friedli, V.; Purrucker, M.; Michler, J. *J. Vac. Sci. Technol., B* **2007**, *25* (6), 2219–2223.

AM1000773